Optimization of Edges in Short Square Pulses in Order to Reduce Shape Distortion

MILAN SIGMUND, LUBOMIR BRANCIK
Brno University of Technology
Department of Radio Electronics
Technicka 12, 61600 Brno
CZECH REPUBLIC
sigmund@feec.vutbr.cz, brancik@feec.vutbr.cz

Abstract: - This paper addresses nanosecond square pulses transmitted by lossy transmission line on conventional printed circuit board. The pulse source is assumed to produce real square pulses with nonzero rise and fall times. Influence of parasitics on the shape is also taken into consideration. Shape distortion of transmitted pulses with duration from 0.1 ns to 10 ns is compared based on the measured transfer function of straight 25 cm long transmission line. For pulses with linear edges, distortion can be reduced using balanced relationship between the rise and fall times. Achievable reduction depends on the duration of the pulse; it is most effective for pulses of 2 ns to 5 ns. The results can be usable in signal processing where we know how much shape distortion can be tolerated.

Key-Words: - shape distortion, square pulse, pulse edges, transmission line on PCB

1 Introduction

Square pulse is the most frequent form of pulses used in standard digital signal processing. Many electronic applications based on signal processing are influenced by the quality of both pulse's excitation and interconnects between electrical modules. As the demand for fast data continuously escalate, the questions arise what happens if the very short square pulse is not ideal (i.e., the transitions on the edge of the pulse is not extremely sharp) and, additionally, if the interconnect transmitting the digital data by means of pulses is also not ideal (i.e., the transmission is not lossless in full frequency range).

Real square pulses in electronic circuits on printed circuit boards (PCBs) differ from the ideal waveform due to limited sharpness of edges and influence of board-based parasitics. Parasitic effects occur more or less depending on physical nature of the used circuit components as well as material of the board and thus, the impact of parasitics should be taken into consideration, especially at high frequencies. Some typical parasitics are described in [1] and formulas for estimation of parasitic capacitance and inductance of individual elements on PCB are presented in [2]. For instance, input of integrated circuits (IC) mounted on PCB is characterized by low serial capacitance (for example, CMOS circuits have typically capacitance of 5 pF). Generally, capacitance of the IC inputs is more significant than capacitance of pins or vias. Remember that some parasitic effects can compensate one another [3], as well as some existing parasitics are simply not effective enough. An overview of basic aspects regarding signal integrity on circuit boards is introduced, for instance, in [4] and [5].

In this study, transmission of very short square pulses by transmission line on conventional PCB was investigated. An introduction to the transmission line theory can be found, for instance, in [6]. Multiconductor transmission lines are studied in [7]. The transmission line itself is usually modelled by cascade connection of the RLGC sections. There are four parameters which specify one section, namely series resistance R, series inductance L, shunt conductance G, and shunt capacitance C. These lumped components are directly related to the electrical parameters of the board materials, such as resistivity and permeability of the trace and conductivity and permittivity of the dielectric. Parameter R models the ohmic losses in the transmission line, while G models the dielectric losses [4]. Thus, a lossless transmission line is characterized by R=0 and G=0. On low-cost PCBs, the line's characteristic impedance can vary as much as ±15% from the target impedance [8]. The RLGC parameters are usually frequency dependent at high frequencies (gigahertz and higher). For instance, the shunt capacitance C is commonly between 0.2-0.8 pF/cm. A frequency dependent RLGC-model up to 20 GHz is described in [9].

Typically, there is a source at one end of the line, and a load at the other end. Figure 1 shows two basic placements of connected source, namely an internal generator mounted directly on the PCB to produce digital data and an external generator delivering for instance clock signal for control. Input of transmission line for external signal is mostly realized by pins that can be source of parasitic capacitances and inductances. Alternatively, external pulses can be received wireless by small size PCB antenna [10], [11].

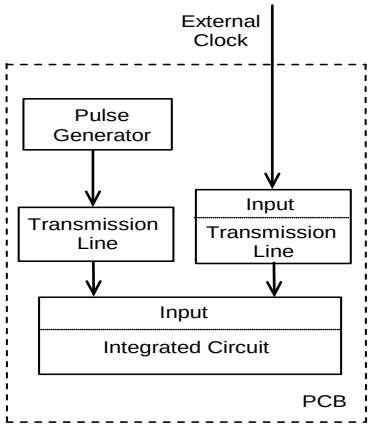

Fig. 1 Schematic connection of transmission lines on PCB for transmission of pulses.

This article is based on the conference paper [12] and provides an extended report of the performed pulse investigation. The rest of the article is organized as follows: Section 2 presents the investigated pulses and analyses their basic spectra, Section 3 gives results of shape distortion under different conditions and, finally, Section 4 makes brief conclusion.

2 Investigated Square Pulses

We have investigated three types of real square pulses from the perspective of distortion by transmission line on a PCB and compared them with the ideal square pulse. All pulses were centered in the time t=0. For our purpose, the waveform of ideal square pulse is defined by two signal levels

$$x(t) = \begin{cases} H & \text{for } |t| \le \vartheta/2 \\ L & \text{otherwise}, \end{cases} \quad (1)$$

where H is high level, L is low level and ϑ denotes the pulse duration. In our experiments, unipolar ideal pulses having the levels L=0 V and H=1 V were taken into account.

The waveforms of real square pulses are based on the ideal pulse but differ in edge characteristics. Figure 2 shows graphically all types of the investigated pulses, namely:

1) ideal square pulse $x(t)$;
2) pulse $x_L(t)$ with linear edges, i.e. pulse generated by real generator assuming negligible parasitics;
3) pulse $x_E(t)$ with exponential edges, i.e. pulse generated by ideal generator but influenced by parasitics;
4) pulse $x_{LE}(t)$ incorporating both effects, i.e. pulse generated by real generator with short linear edges and then influenced by parasitics on the board.

Note that the pulses are referred to as square pulse with linear or exponential edges (and not trapezoidal or exponential pulse) with respect to the fact that an edge usually represents a very short portion of the full width of the pulse. For comparison purposes, all pulses shown in Fig. 2 were regarded symmetric from –0.5 s to 0.5 s having unity height 1 V and unity width 1 s. Most of real signals carrying digital data are typically modelled by pulses with equal rise time t_R and fall time t_F. Hence, our analysis of square pulses is first focused on signals having also equal times t_R=t_F.

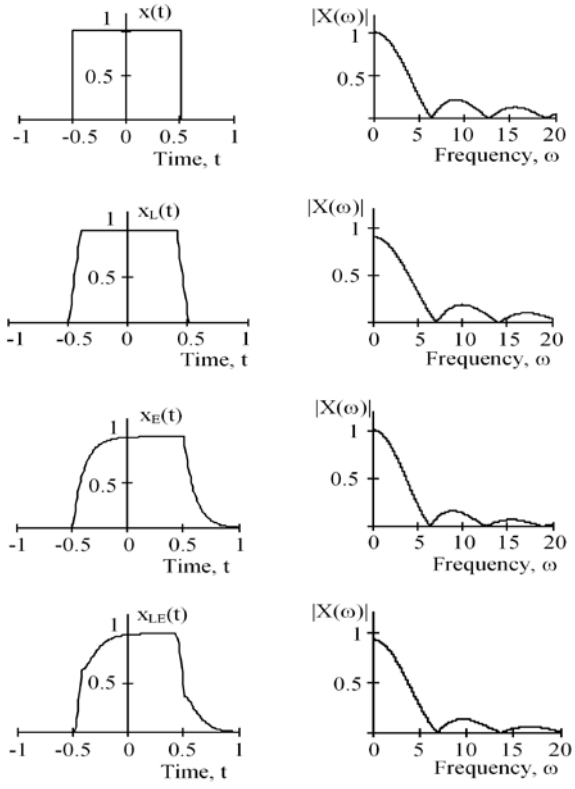

Fig. 2 Waveforms (left column) and continuous spectra (right column) of investigated pulses.

To determine the signal spectrum $X(\omega)$, standard Fourier transform [13] was applied

$$X(\omega) = \int_{-\infty}^{\infty} x(t) \exp(-j\omega t)\, dt\,, \tag{2}$$

where $x(t)$ is signal in time domain (here the pulse waveform), ω is circular frequency, and j stands for imaginary unit. For the ideal square pulse (1), transform (2) goes into a simpler form

$$X_{\mathrm{ID}}(\omega) = H\,\vartheta\,\frac{\sin(\omega\,\vartheta/2)}{\omega\,\vartheta/2}. \tag{3}$$

Another simplified specific formula results for real pulses having linear edges with the same rise and fall times $t_R=t_F\rightarrow t_{RF}$

$$X_{\mathrm{L}}(\omega) = H(\vartheta - t_{\mathrm{RF}})\,\frac{\sin(\omega\,(\vartheta - t_{\mathrm{RF}})/2)}{\omega\,(\vartheta - t_{\mathrm{RF}})/2}\,\frac{\sin(\omega\,t_{\mathrm{RF}}/2)}{\omega\,t_{\mathrm{RF}}/2} \tag{4}$$

which contains product of three expressions; two of them are similar ratios. The first ratio depends on the difference between pulse width ϑ and edge time t_{RF} while the second one depends on the edge times t_{RF} only. By using the important property for limit $\alpha\rightarrow 0$ of general $\sin(\alpha)/\alpha$ function

$$\lim_{\alpha\to 0}\frac{\sin(\alpha)}{\alpha} = 1\,, \tag{5}$$

formula (4) is reduced to (3) when $t_{RF}=0$ in (4), i.e. the rise and fall times are zero.

For a proper understanding of the pulse spectrum, we have studied more in details the effect of varying edge slope on spectrum of the pulse with linear edges and exponential edges, respectively. In Fig. 3, the results for edge durations t_{RF} representing 0% (i.e. ideal square pulse), 5%, and 10% of the full pulse width are graphically compared. Each of the waveforms is symmetric to t=0 (i.e., satisfies an even function), so the Fourier spectrum results only in real part values. All spectra are displayed for low frequencies from 0 to 8π which cover approximately the four most energy significant spectral lobes. For these pulses, increasing rise and fall times influence the spectrum in two ways: peaks of all individual lobes (i.e., local spectral maxima) are lower and zero points are shifted from multiples of 2π to higher frequencies. Thus, the whole spectrum becomes flatter. Decrease of the main peak at the frequency ω=0 with growing edge time t_{RF} is given by a simple relation. This peak is determined only by the first expression in (4)

$$X_{\mathrm{L}}(0) = H(\vartheta - t_{\mathrm{RF}}) \tag{6}$$

because for the frequency ω=0 is equation (4) reduced to (6) according to the property (5).

Regular zero points in the spectrum are given by zero values in the sinus function, specifically

$$\sin\frac{\omega\,(\vartheta - t_{\mathrm{RF}})}{2} = 0\,. \tag{7}$$

This is true when the argument of sinus goes to a multiple of π, which are frequencies

$$\omega_z = \frac{2k\pi}{\vartheta - t_{\mathrm{RF}}} \tag{8}$$

where k stands for natural numbers. For t_{RF}=0 and ϑ=1, all zero points are located at frequencies of the exact multiples of 2π. Any parameter $t_{RF}\neq 0$ shifts all the zero points ω_z to higher values. In addition, the last expression in (4) produces other zero points in a similar way

$$\omega_{zz} = \frac{2k\pi}{t_{\mathrm{RF}}}\,. \tag{9}$$

In the situation shown in Fig. 3, the lowest zero point of this type corresponds to t_{RF}=10% (i.e, t_{RF}=0.1 s) and has the circular frequency $\omega_{zz}=20\pi$; therefore, it lies beyond the scope of the spectral graph.

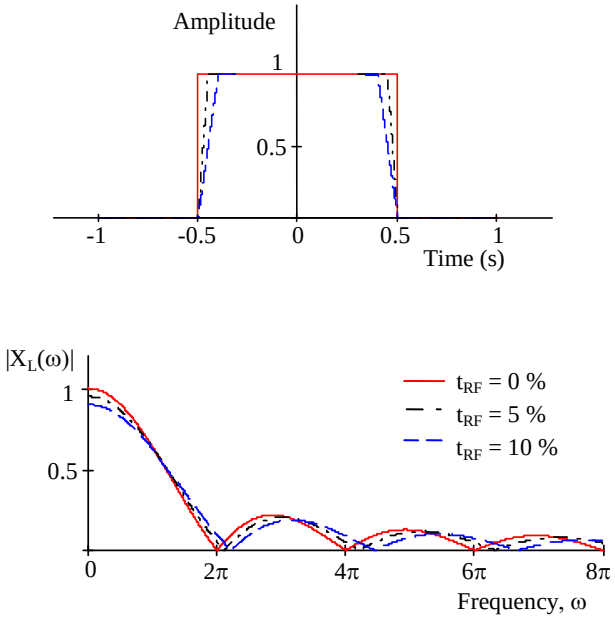

Fig. 3 Detail waveforms (top) and corresponding spectra (bottom) of pulses with different linear edges when $t_R=t_F=t_{RF}$.

Further, waveforms and corresponding spectra for the pulses having exponential edges with time constants of 0%, 5%, and 10% of the full pulse width are shown in Fig. 4. Each pulse has equal time constants $\tau_R=\tau_F\rightarrow\tau_{RF}$ for rise and fall edges. Since the waveform of these pulses is not fully symmetric to t=0, the Fourier spectrum results in complex values. For comparison, the spectra in Fig. 4 are displayed in the same frequency range as in Fig. 3. Unlike the pulses with linear edges in Fig. 3, this spectrum shows to be much more robust against the change in edge time. Only peaks of the side lobes are influenced—they decrease with growing edge time while the peak of the main lobe is not changed as well as the main lobe has in all cases nearly the same slope, independently of the time constants. Furthermore, all the zero points in spectrum remain at the origin frequencies given by the multiples of 2π (in this case). There are no additional zero points as in previous pulse type.

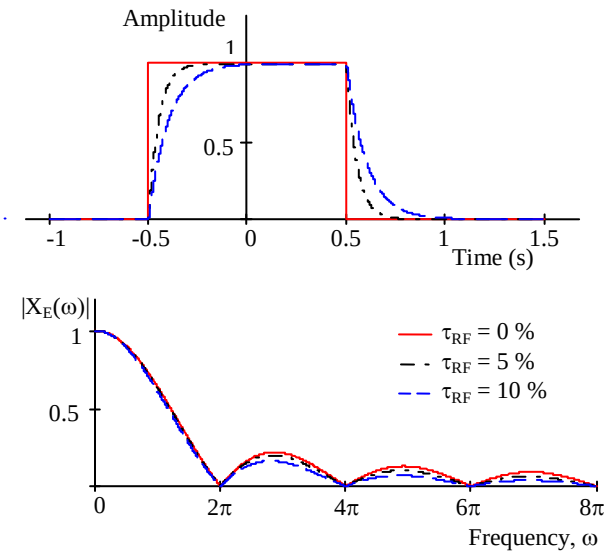

Fig. 4 Detail waveforms (top) and corresponding spectra (bottom) of pulses with different exponential edges when $\tau_R=\tau_F=\tau_{RF}$.

3 Obtained Results

Pulse analysis focuses on the shape distortion of the pulse types presented in Section 2 due to frequency limited transmission by the transmission lines on PCB. The shape distortion (in percent) was estimated in time domain as ratio of the pulse areas

$$D=\frac{\int_{-\infty}^{\infty}|x(t)-y(t)|dt}{\int_{-\infty}^{\infty}|x(t)|dt}100 \qquad (10)$$

where $x(t)$ is the original pulse before transmission and $y(t)$ stands for the same pulse distorted by transmission. The symbol $x(t)$ represents in computation (10) all types of pulse, i.e. $x(t)$, $x_L(t)$, $x_E(t)$, and $x_{LE}(t)$, respectively. All pulses $x(t)$ as well as $y(t)$ were centered at time t=0 in order to eliminate influence of transfer delay. Only changes in the pulse form are taken into account in the computation. Other definition of pulse distortion based on total harmonic distortion can be found in [14], for instance. Generally, for the degree of shape distortion plays key role the relationship between two frequency bandwidths: the bandwidth of the transmission line and the bandwidth of the pulse signal that is carried by the transmission line. Because of the line's bandwidth is more or less predetermined, for example, by the line geometry or by the PCB material and topology, so the relationship can be optimized only by the bandwidth of pulse spectrum.

In the following experiments, the time parameters t_R, t_F, and ϑ were measured on waveforms as is illustrated in Fig. 5.

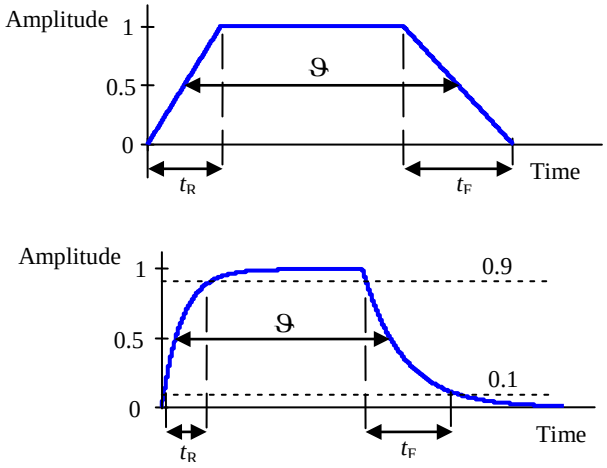

Fig. 5 Definition of time parameters in pulses with linear edges (top) and exponential edges (bottom).

The pulse duration was measured in all types of investigated pulses on the 50% level of the pulse height H. The measurement of the edge times differs depending on type of the pulse. In pulses with nonlinear edges, i.e. $x_E(t)$ and $x_{LE}(t)$ are t_R and t_F defined as time interval between the points where the appropriate edge achieves 10% and 90% of the pulse height H, while in pulse with linear edges, i.e. $x_L(t)$ represent t_R and t_F entire duration of the respective edge (in ideal pulse is the edge duration zero).

3.1 Transfer Characteristics of Microstrip Line on Conventional PCB

In order to obtain detailed view on signal transfer, we have measured the transfer characteristics of parallel coupled microstrip lines on a PCB without mounted electrical components. The straight transmission lines were 25 cm long, 1 mm width and 35 μm thick with distance between lines of 6 mm. The board was made from the substrate FR4 (fiberglass) 1.5 mm thick with relative permittivity of $\varepsilon_r = 4.3$. Fig. 6 shows the transfer function measured by network analyzer Agilent E5071C in frequency range from 300 MHz to 10 GHz and its approximation in full frequency band from 0 to 10 GHz. It is clearly evident that the transfer function meets low-pass filter function. High frequencies above about 7.5 GHz are practically not transmitted. On the other hand, frequencies below 300 MHz are not affected and frequencies in the band from 300 MHz to 1 GHz are only slightly damped. The basic theory of low-pass filtering of pulse signals can be found, for instance, in [15]. The approximate curve in Fig. 5 resulted from the measured data using the minimum total error criterion [16] by examination of the squared pointwise errors between the measured and the approximated curve.

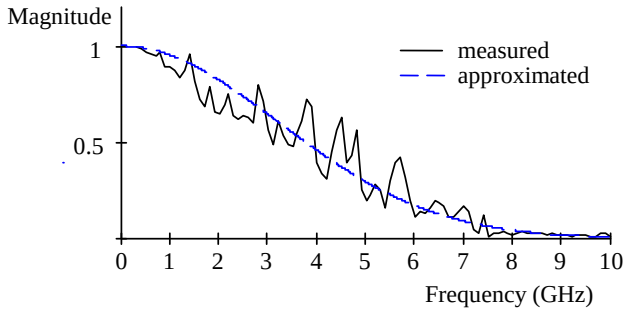

Fig. 6 Transfer function of 25 cm long transmission line on PCB.

Based on the approximate curve, the theoretical cut-off frequency was set to $F_{CO} = 2.615$ GHz which corresponds to the value of 0.707 (i.e., –3 dB) at the curve. Figure 7 illustrates the waveforms of transmitted 1 ns pulse along with the original pulse using either the theoretical low-pass filter (passing the frequencies from 0 to F_{CO} and rejecting other frequencies) or the real low-pass filter according to the nonlinear approximate curve (dashed line in Fig. 6). The loss of high-frequency components contained in short square pulses logically makes a flattening of the sharp edges. By applying the ideal low-pass, the waves oscillate which, in addition, increases the overall distortion. Thus, the approximate transfer function was used in next experiments for estimation of exact pulse's distortion.

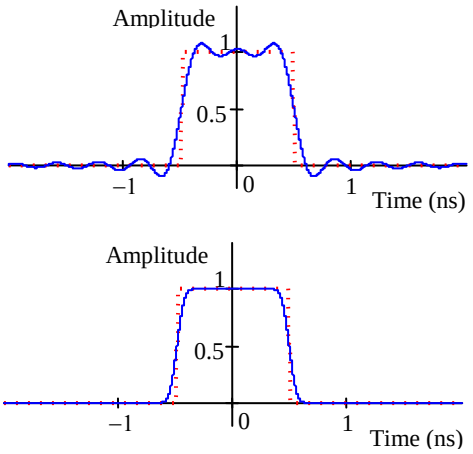

Fig. 7 Comparison of 1 ns pulse with 1% edge duration applying the transfer function once as theoretical low-pass filter (top) and once as real low-pass filter (bottom). Dotted lines show original pulses before transmission, solid lines are pulses after transmission.

3.2 Distortion of Pulses during Transmission

We have investigated shape distortion of the real square pulses $x_L(t)$, $x_E(t)$ and $x_{LE}(t)$ as well as the ideal square pulse $x(t)$ when passing through transmission line. All pulses were observed in the nanosecond regime with pulse duration from 0.1 ns to 2 ns and two different edge times: 1% and 5% of the full pulse duration (except for the ideal pulse having zero edges). In each pulse, the rise and fall times were equal.

To get an overview of the distortions, obtained results are summarized in Table 1 and Table 2 separately for both mentioned edge times. The first row presenting the distortion of the ideal square pulse $x(t)$ shows the same results in both tables, because in this pulse the edge time is always zero. In nanoseconds, distortion was more dependent on pulse duration and less on impulse type. Distortion of the pulse with purely exponential edges $x_E(t)$ seems to be similar to the distortion of Gaussian pulse [17]. Comparing Tables 1 and 2, it can be seen

that the pulses with sharper edges (Table 1) are more distorted by the filtering effect of the transmission line. Regardless of the edge slope, the use of pulses shorter than 0.6 ns can be problematic particularly in signal processing on conventional PCBs (such as the measured board) due to their high deformation.

TABLE 1 PULSE DISTORTION (IN PERCENT) WHEN EDGE SLOPE COVERS 1% OF PULSE DURATION

Pulse form	Pulse duration (ns)				
	2	1	0.6	0.3	0.1
$x(t)$	4.1	8.1	13.4	26.7	77.8
$x_L(t)$	3.3	7.3	12.7	26.1	78.2
$x_E(t)$	2.7	6.4	11.6	24.7	76.7
$x_{LE}(t)$	2.3	5.5	12.5	26.2	76.6

TABLE 2 PULSE DISTORTION (IN PERCENT) WHEN EDGE SLOPE COVERS 5% OF PULSE DURATION

Pulse form	Pulse duration (ns)				
	2	1	0.6	0.3	0.1
$x(t)$	4.1	8.1	13.4	26.7	77.8
$x_L(t)$	1.7	5.8	10.1	24.8	79.9
$x_E(t)$	1.2	3.5	7.5	19.0	68.6
$x_{LE}(t)$	1.4	3.4	6.7	17.1	77.2

TABLE 3 DISTORTION AGAINST IDEAL SQUERE PULSE FOR 1 NS PULSES WHEN EDGE SLOPE COVERS 5% OF PULSE DURATION

Pulse form	Shape distortion (%)	
	Before transmission	After transmission
$x(t)$	0	8.08
$x_L(t)$	10.02	12.55
$x_E(t)$	14.41	16.99
$x_{LE}(t)$	19.48	22.82

Another way to compare pulse distortion by the transmission line is shown in Table 3. Here are compared the shape distortions in all types of pulse against ideal pulse before and after transmission. In this way, distortion caused by transmission appears to be less than the distortion of the same pulses measured regardless of the ideal pulse (compare with the column for 1 ns pulse in Table 2). Table 3 presents the results for 1 ns pulses, but a similar trend is also seen with pulses of different duration.

As can be seen in Tables 1 and 2, pulses of 0.1 ns are significantly deformed during the transmission along the whole waveform. In comparison with their initial waveform they do not achieve the original height of 1 V at all and they are rounded as well as spread in time. Figure 8 illustrates the shape deformation of 0.1 ns pulses when each edge time t_R and t_F is 10% of the full pulse duration, i.e. t_R=t_F=10 ps. In this case, achieved peaks are below 0.7 V. The decrease of the peak begins to show in pulses shorter than 0.3 ns and drops nonlinear when the pulses are further shortened. Figure 9 shows decrease of peak for pulses with duration from 0.1 ns to 0.3 ns having constant edge time of 10 ps and 20 ps, respectively. Pulses with linear edges are more affected by the drop of peak as pulses with exponential edges. To maintain 99% of the original peak, the pulses must not be shorter than 0.26 ns.

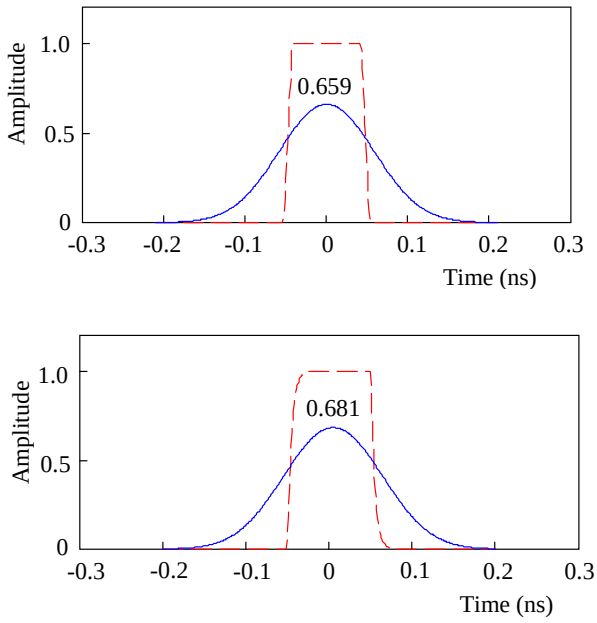

Fig. 8 Deformation of 0.1 ns pulses with linear edges (top) and with exponential edges (bottom). Dashed lines show original pulses before transmission, solid lines are deformed pulses after transmission.

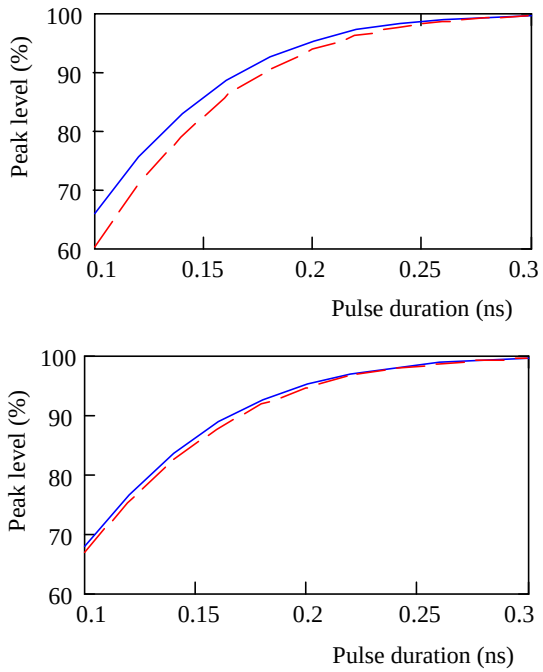

Fig. 9 Drop of peak in very short pulses with linear edges (top) and with exponential edges (bottom). Solid line is for edge time 10 ps, dashed line is for edge time 20 ps.

3.3 Reduction of Distortion by Optimization of Edge Relation

In next experiments, we have estimated how the distortion depends on the relation of rise time t_R to fall time t_F when the sum of both times t_R+t_F retains constant. For pulses $x_L(t)$, the shape distortion slightly decreases to the minimum that it achieves when the edge times are equal $t_R=t_F$. An example of the symmetric dependence of distortion is depicted in Fig. 10 for the pulse of 1 ns keeping the t_R+t_F sum to 10% of the full pulse duration (i.e., 100 ps). The relation t_R to t_F varies from 0:10 to 10:0, i.e. the rise time t_R grows from 0 up to 10% and the fall time t_F vice versa. Such a dependence did not occur in pulses with exponential edges, i.e. $x_E(t)$ and $x_{LE}(t)$.

The total reduction as the difference between the maximum and minimum distortions in each pulse (i.e., change of t_R:t_F from 0:10 to 5:5 or 10:0 to 5:5) depends on the duration of the pulse. Figure 11 shows an overview of distortion reductions for pulses with duration from 0.1 ns to 10 ns having the t_R+t_F sum of 10% of the pulse duration. The best improvement about 0.5% was achieved for pulses with duration between 2 ns and 5 ns. Still, a small reduction in distortion is important. For example, in 5 ns pulse, the distortion has decreased from 1.04% to 0.49%.

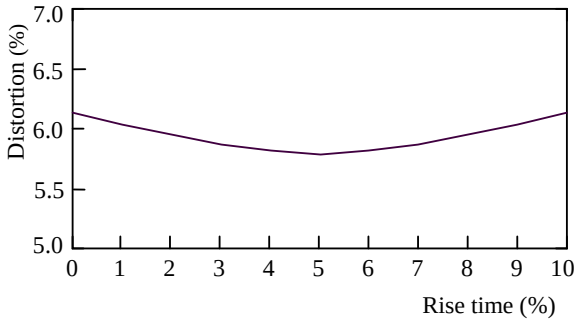

Fig. 10 Evolution of the shape distortion dependent on the relation t_R to t_F when t_R+t_F=10%: example for 1 ns pulse.

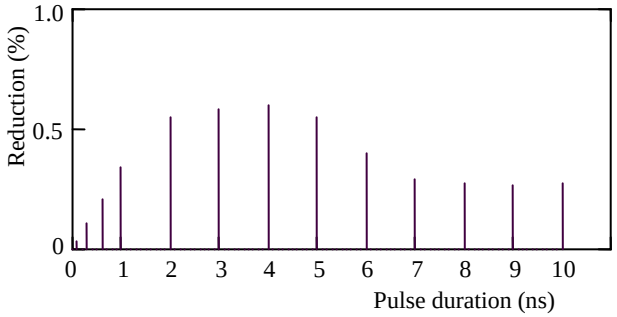

Fig. 11 Achievable reduction of shape distortion versus pulse duration.

4 Conclusion

Single square pulses in nanosecond regime were objects of this study focused on shape distortion of the pulses by conventional transmission line on PCB. The shorter the single pulse, the higher possible speed of pulse series as well as speed of periodic signal created by repeating the pulse. The transmission lines can transmit signals in the frequency band up to low gigahertz. If higher frequencies are needed, other technologies should be considered such as printed "coaxial-like" transmission line [18] or optical signals [19]. However, these alternatives are a bit more expensive solutions. Signal analysis leading to the results in this paper was implemented using Mathcad [20]. Presented theory and results can help to better understand some frequency effects limiting practical signal processing on PCB using square pulses. For a complete view, let's say other effects that can deform very short pulses on PCB such as crosstalk [6] and electromagnetic radiation [21].

Acknowledgments

Research described in this paper was financed by Czech Ministry of Education in frame of National Sustainability Program under grant LO1401. For research, infrastructure of the SIX Center was used. The research was also financially supported by the Brno University of Technology Internal Grant Agency under project no. FEKT-S-17-4707.

References:

[1] I. Erdin and R. Achar, Small Signal AC Analysis of Controller Circuits with Distributed PCB Effects, in *Proc. Asia-Pacific International Symposium on Electromagnetic Compatibility*, Shenzhen, China, 2016, pp. 1150-1152.

[2] T. Le Gouguec, et al., Modelling up to 45 GHz of Coupling between Microvias and PCB Cavities Considering Several Boundary Conditions, *International Journal of Microwave and Wireless Technology*, Vol.8, No.3, pp. 421-430, May 2016.

[3] J. Jerabek, J. Dvorak, R. Sotner, B. Metin, and K. Vrba, Multifunctional Current-Mode Filter with Dual-Parameter Control of the Pole Frequency, *Advances in Electrical and Computer Engineering*, Vol.16, No.3, pp. 31-36, August 2016.

[4] S. C. Thierauf, *High-Speed Circuit Board Signal Integrity*, 2nd edition, Boston, London: Artech House, 2017.

[5] M. Li, *Jitter, Noise, and Signal Integrity at High-Speed*. Upper Saddle River: Prentice Hall, 2007.

[6] C. R. Paul, *Transmission Lines in Digital and Analog Electronic Systems: Signal Integrity and Crosstalk*, Hoboken, NJ: John Wiley, 2011.

[7] C. R. Paul, *Analysis of Multiconductor Transmission Lines*. New York: John Wiley & Sons, 2008.

[8] S. H. Hall, G. W. Hall, and J. A. McCall, *High-Speed Digital System Design*, New York: John Wiley, 2000.

[9] T. Liang, S. Hall, H. Heck, and G. Brist, A Practical Method for Modeling PCB Transmission Lines with Conductor Surface Roughness and Wideband Dielectric Properties, in *Proc. IEEE MTT-S International Microwave Symposium Digest*, San Francisco, CA, 2006, pp. 1780-1783.

[10] Z. Chen and Y. P. Zhang, FR4 PCB Grid Array Antenna for Millimeter-Wave 5G Mobile Communications, in *Proc. IEEE MTT-S Int. Microwave Workshop Series on RF Wireless Technologies for Biomedical and Healthcare Applications (IMWS-BIO)*, pp. 1-3, Singapore, December 2013.

[11] Y. Yin, B. Zarghooni, and K. Wu, Single-Layered Circularly Polarized Substrate-Integrated Waveguide Horn Antenna Array. *IEEE Transactions on Antennas and Propagation* Vol.65, No.11, pp. 6161-6166, November 2017.

[12] M. Sigmund and L. Brancik, Distortion of Short Square Pulses by Transmission Line on Printed Circuit Board, in *Proc. European Conf. on Electrical Engineering and Computer Science (EECS 2017)*, Bern, Nov. 2017, to be published.

[13] K. Gröchenig, *Foundations of Time-Frequency Analysis*, New York: Springer, 2013.

[14] B. Dobrucky, O.V. Chernoyarov, and M. Marcokova, Computation of the Total Harmonic Distortion of Impulse System Quantities Using Infinite Series, in *Proc. 14th Conference on Applied Mathematics*, Bratislava, 2015, pp. 213-220.

[15] E. W. Kamen and B. S. Heck, *Fundamentals of Signal and Systems*, Upper Saddle River, NJ: Pearson Prentice Hall, 2007.

[16] W. J. Welch, A Mean Squared Error Criterion for the Design of Experiments, *Biometrika*, Vol.70, No.1, pp. 205-213, April 1983.

[17] M. Sigmund and L. Brancik, Requirements on Needed Frequency Bandwidth Depending on Pulse Waveforms and their Allowed Distortion, *Journal of Electrical Engineering*, Vol.67, No.6, pp. 459-462, December 2016.

[18] J. S. Izadian, J. Ferry, and J. McAllister, Novel Transmission lLne for 40 GHz PCB Applications, in *Proc. DesignCon*, Santa Clara, CA, 2011, Vol.2, pp. 1390-1412.

[19] J. Yu, X. Li, and J. Zhang, *Digital Signal Processing for High-Speed Optical Communication*, World Scientific, 2018.

[20] B. Maxfield, *Engineering with Mathcad: Using Mathcad to Create and Organize your Engineering Calculations*, Amsterdam: Elsevier, 2006.

[21] A. M. Sayegh, M. Z. B. Jenu, S. Z. Sapuan, and S. H. B. Dahlan, Analytical Solution for Maximum Differential-Mode Radiated Emissions of Microstrip Trace, *Trans. on Electromagnetic Compatibility*, Vol.58, No.5, pp. 1417-1424, May 2016.